ELSEVIER

NeuroImage

www.elsevier.com/locate/ynimg
NeuroImage 41 (2008) 914–923

Automatic localization and labeling of EEG sensors (ALLES) in MRI volume

L. Koessler,[a,b,c] A. Benhadid,[a,b] L. Maillard,[b,c] J.P. Vignal,[c] J. Felblinger,[a,b] H. Vespignani,[b,c] and M. Braun[a,b,d,*]

[a]*INSERM ERI13, Nancy, France*
[b]*Nancy University, Nancy Brabois, France*
[c]*Neurology Department, University Hospital, Nancy, France*
[d]*Neuroradiology Department, University Hospital, Nancy, France*

Received 28 August 2007; revised 4 February 2008; accepted 14 February 2008
Available online 6 March 2008

Spatial localization of scalp EEG electrodes is a major step for dipole source localization and must be accurate, reproducible and practical. Several methods have been proposed in the last 15 years. The most widely used method is currently electromagnetic digitization. Nevertheless, this method is difficult to use in a clinical environment and has not been validated with a high number of electrodes. In this paper, we introduce a new automatic method for localizing and labeling EEG sensors using MRI. First, we design a new scalp EEG sensor. Secondly, we validate this new technique on a head phantom and then in a clinical environment with volunteers and patients. For this, we compare the reproducibility, accuracy and performance of our method with electromagnetic digitization. We demonstrate that our method provides better reproducibility with a significant difference ($p<0.01$). Concerning precision, both methods are equally accurate with no statistical differences. To conclude, our method offers the possibility of using MRI volume for both source localization and spatial localization of EEG sensors. Automation makes this method very reproducible and easy to handle in a routine clinical environment.

Keywords: Electroencephalography (EEG); Magnetic resonance imaging (MRI); Source localization; EEG-MRI sensor; ALLES

Introduction

Recent developments (in the 1990s) in electroencephalographic (EEG) source imaging have made it possible to localize brain generators using information on the electrical field recorded on the surface of the head (Michel et al., 2004). Important applications of this non-invasive method include investigation of partial epilepsy (Gavaret et al., 2004, 2006; Huppertz et al., 2001), and event related potentials (ERP) (Alary et al., 1998, Thees et al., 2003). The strength of EEG source localization is co-registration of electroencephalographic data and magnetic resonance images (MRI). This allows two different kinds of information to be combined, i.e. temporal information with a time scale in the order of a millisecond with EEG, and anatomical information on a scale in the order of a millimeter, with MRI.

The visual inspection of EEG traces, in standard clinical use, is difficult to correlate with anatomical structures. However, EEG source imaging permits accurate correlation of EEG information with anatomical structures in the brain. In order to localize the source, three different elements are required: a high resolution MRI volume, a high resolution EEG (high sampling rate and large number of electrodes) and the 3D coordinates of the EEG electrodes. Accurate localization of the EEG sensors is necessary for precise definition of brain generators. Usually a fiducial landmark (nasion, left and right ears) is set to define a reference frame for location of the sensors. In this way, it is possible to co-register the EEG data with the MRI volume. However, if errors are made in the electrode's location this will have a knock-on effect on the position of the brain generator observed (Khosla et al., 1999).

Several different methods have been suggested for accurately locating the EEG electrodes (reviewed in Koessler et al., 2007).

While some are manual (De Munck et al., 1991; Le et al., 1998), the commonest techniques use electromagnetic digitizers (Gevins et al., 1990; Wang et al., 1996; Le et al., 1998; Khosla et al., 1999). Other works propose alternative methods: MRI localization of the electrodes (Lagerlund et al., 1993; Yoo et al., 1997; Brinkmann et al., 1998; Sijbers et al., 2000), the use of the geodesic photogrammetry system (GPS) (Russell et al., 2005; Tucker, 1993), and the use of ultrasound digitization (Steddin and Bötzel, 1995).

The spatial localization of EEG electrodes needs to be accurate, fast, reproducible and adapted to clinical use (Le et al., 1998). However,

* Corresponding author. INSERM ERI13, Nancy, France. Fax: +33 383 852 236.
E-mail address: m.braun@chu-nancy.fr (M. Braun).
Available online on ScienceDirect (www.sciencedirect.com).

1053-8119/$ - see front matter © 2008 Published by Elsevier Inc.
doi:10.1016/j.neuroimage.2008.02.039

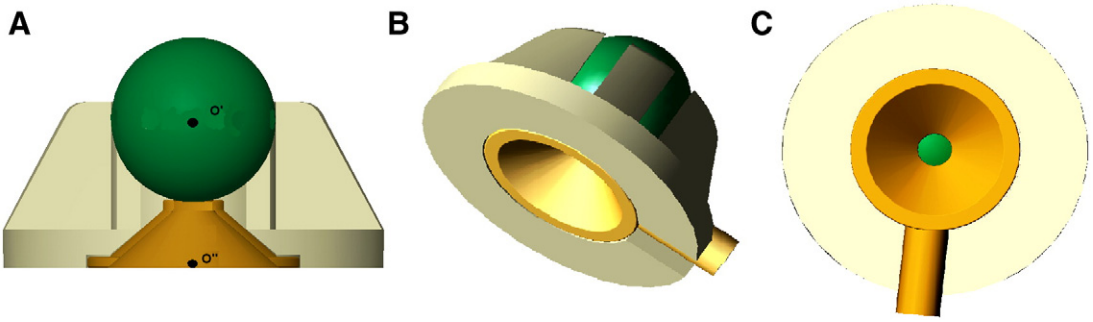

Fig. 1. Cross-section (A), lateral (B) and bottom view (C) of the EEG-MRI sensor.

the precise level of accuracy necessary or meaningful for surface electrode localization is unclear. In fact, the accuracy of the spatial localization of the EEG electrode is just a parameter among many others which can influence source localization (Wang and Gotman, 2001; Lantz et al., 2003). According to the literature, precision of less than 5 mm is necessary for dense arrays of electrodes and a source inversion algorithm (Brinkmann et al., 1998). Of the various techniques proposed, spatial localization of EEG electrodes with MRI is the approach most appropriate to the source localization problem, since it does not require additional materials and experienced users. Furthermore, the MRI data can be used to infer a realistic model of the head which would help in very accurately localizing the source generator (Sijbers et al., 2000; Koessler et al., 2007).

Few automatic algorithms designed to localize EEG sensors in MRI volume data have previously been described (Sijbers et al., 2000; Yoo et al., 1997; Wang et al., 1996). The surface matching algorithms among them have been shown to be robust and accurate in many applications (West et al., 1997). All of these methods used morphological operations (opening, closing, dilatation, erosion etc.) to detect EEG sensors, but these algorithms were not successful in clinical practice due to the lack of dedicated EEG sensors and the difficulty in labeling the electrodes on the MRI data.

In this paper, we describe an automatic method for detecting and labeling new scalp-recorded EEG sensors in MRI volume data. The accuracy of the technique is compared with the electromagnetic digitization method. The algorithm was developed with the purpose of reducing the operator's time and possible human errors in the localization process. The new EEG sensor is MR compatible, i.e. no susceptibility artifact on the MR images or induced currents that could harm the subject, and it is MR localizable. With this new method, only two different examinations (EEG and MRI) are required to localize the source, without additional materials being needed.

Materials and methods

EEG/MRI sensors

The new EEG sensor was made by combining four different elements (Fig. 1): (i) a 10 mm diameter Ag/AgCl EEG electrode (Medical Equipment International, Montreuil, France), (ii) a support

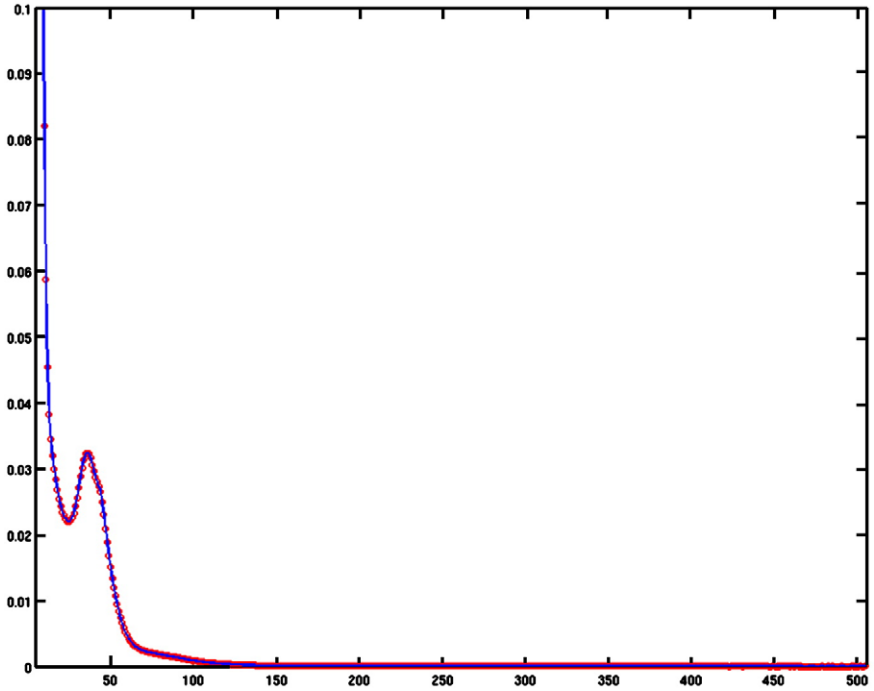

Fig. 2. Curve fitting of the histogram of the MRI volume and automatic thresholding.

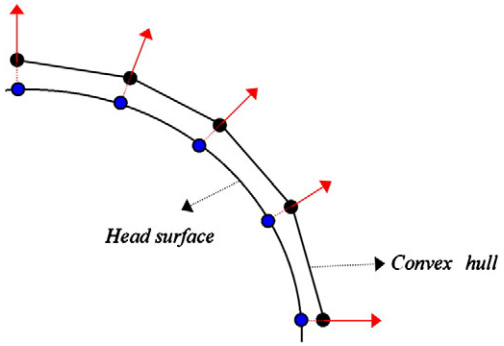

Fig. 3. Example of a head surface which shows how the projection of markers coordinates.

designed to hold an MRI marker, (iii) an MRI marker consisting of an 8 mm diameter gadolinium ball (BrainLab, Heimstetten, Germany) and (iv) a short cable (about 5 cm) for connecting to the EEG acquisition system. The complete sensor with its short wire reduces the possibility of producing a loop in the MR scanner and thus reduces the risk of induced currents. The ergonomic support is 8 mm in height and 18 mm wide and does not cause any discomfort to the subject. Several ferro-magnetism MR tests have been carried out using T1, T2 and EPI sequences and have validated the MR compatibility and safety of the sensor.

MRI data acquisition

All MRI examinations were performed on a 1.5T GE Signa (GE Healthcare, Milwaukee, WI) with an eight element coil. During the process, special care was taken so that neither the scalp nor any of the sensors moved. The parameters of the MR sequence were selected for both accurately detecting the EEG sensors and producing precise anatomical brain images. Contrasted high resolution 3D MRI acquisition was chosen to show possible cortex abnormalities and to produce correct gray and white matter differentiation.

Additionally, the complete MR procedure was performed fast enough to avoid discomfort to the subject and reduce artifacts caused by motion. To do this, we used a 3D Spoiled Gradient Echo sequence (TR=20 ms, TE=3 ms, α=35°) with 230 mm field of view, 192 × 192 matrix, and 200 slices. Slice thickness was 1.2 mm without any gap between slices. A large bandwidth (31.2 kHz) was used to reduce distortion due to magnetic susceptibility.

Automatic localization and labeling of the EEG sensor (ALLES)

To carry out automatic labeling and identification of EEG electrodes using MRI, we consider that the surface of the human head is convex, except for the cavities around the eyes. We can therefore expect the positions of the EEG electrodes on the scalp to form a convex cloud of points, i.e. the EEG electrodes are part of the convex hull defined by the scalp. This gives an idea of how EEG electrodes can be identified in the MRI volume.

First, a 3 × 3 median filter is applied to the MRI volume in order to smooth away noisy voxels, and obtain a homogeneous MRI volume for further processing. The next step in the algorithm fits an adaptive cubic spline curve to the histogram of the MRI volume for automatic thresholding of the hypersignals associated with the gadolinium balls (Fig. 2). Indeed, the histogram of the MRI volume of the head shows a lobe corresponding to the voxels occupied by the volume of the head and a very high peak for low level intensities associated with the background. The intensity of the hypersignals associated with the gadolinium balls extends along the space right of the lobe in the histogram. The threshold for the gadolinium balls is set at a position where the maximum in absolute value between the slope of the spline and its curvature is less than 0.001, i.e. $\max(|\text{spline}_{\text{slope}}|, |\text{spline}_{\text{curvature}}|) < 0.001$. That is, the threshold is set where the spline fit becomes an almost straight line parallel with the x-axis (Fig. 2). The spline curve is obtained using the curve fitting toolbox of Matlab. The thresholding at this position of the histogram permits segmenting out all data associated with the subject's head and background. The EEG sensor signals from the head could then be separated.

Furthermore, in order to get rid off spurious voxels due to abrupt thresholding, the volume is cleaned up using morphological operations (Heijmans, 1994). This task was carried by applying an opening operation using a sphere structure element with radius equal to 2 mm. A radius in this range ensures that the hypersignals associated with the gadolinium balls in the MRI volume are not erased.

The second part of the algorithm constructs a Delaunay convex hull (Boissonnat and Teillaud, 1986; Ernst et al., 1996) using the barycenters of the automatically detected gadolinium balls. This helps to eliminate any spurious detection of gadolinium balls located inside the patient's head. Lastly, the 3D coordinates of the convex hull vertices (the marker) need to be corrected to obtain the right coordinates of the EEG sensors. To accomplish this task, we first need to estimate the normals to the convex hull (Fig. 3). The normal to the hull at a given barycenter $Vi(xi,yi,zi)$ is estimated as follows: first, we define a sphere, having a small arbitrary radius, centered at Vi, and then we look for the list of intersection points $\{Pi\}$ of this sphere with the mesh around the point Vi. As the intersection points $\{Pi\}$ would lie approximately on a same plane which is tangent to the convex hull at the barycenter Vi (Guofei et al., 2005), one can use the Principal Component Analysis (PCA) technique to estimate the plane that fits the points $\{Pi\}$, and consequently obtain the normal vector $Ni=(ai, bi, ci)$ to that plane. Secondly, since a surface plane has two possible normals pointing to opposite directions, we choose to make the estimated normals pointing outwards. This is done by observing a positive distance di between the barycenter Vi and the surface defined by the normal Ni at the origin of the MRI volume, i.e. $di=ai * xi+bi * Vi+ci * zi>0$. It is worth mentioning that the above trick is possible since the origin of the MRI volume is inside the convex hull. Indeed, a

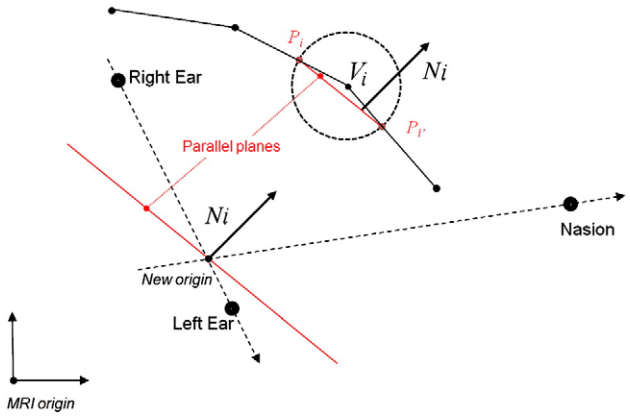

Fig. 4. Correction of the EEG sensor coordinates (Vi).

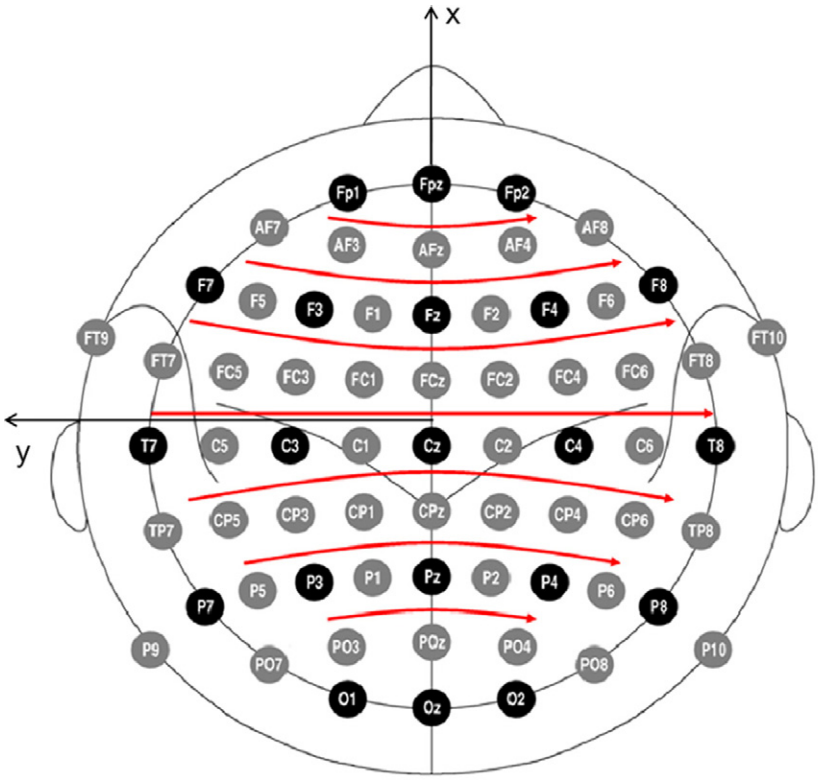

Fig. 5. Black circles indicate positions of the original 10/20 system, grey circles indicate additional positions introduced in the 10/10 extension (adapted from Oostenveld et al., 2001). Red arrows show the procedure of labelling EEG sensors.

coordinate transform is applied to the MRI volume in order to shift the origin of the volume to the point (0.0.0) defined by the anatomical landmarks (nasion, left and right ears) (Fig. 4). Finally, the correction to the coordinates of *Vi* is carried by adding a small distance (8 mm) in the opposite direction to the normal.

The third and final stage of the algorithm projects the estimated locations of the EEG electrodes onto an ellipsoid that models the patient's head. After readjusting to align the ellipsoid with the ten–ten international system, the EEG electrodes can be automatically labeled. First, the four basal temporal electrodes (FT9, P9, FT10, and P10) are sorted according to their *x*–*y* coordinates, and then labeled accordingly. Afterwards, the outer ring is labeled, working clockwise and starting from the electrode Fpz. The remaining electrodes are sorted into seven sets of electrodes with respect to their *y* coordinates. The first and last sets contain only three electrodes each, while the other sets have seven electrodes each. The electrodes in the sets are labeled from left to right (Fig. 5).

Finally, the algorithm writes the list of EEG electrode coordinates estimated in a file to be used with the source localization software. It is worthy of mention that the projection stage is only performed for

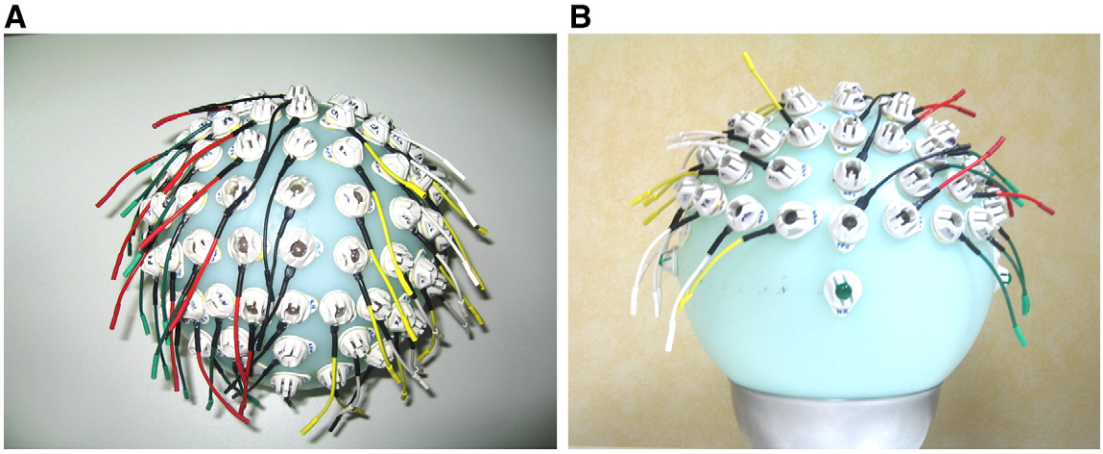

Fig. 6. Top (A) and front (B) views of 64 sensors taped on the MRI head phantom.

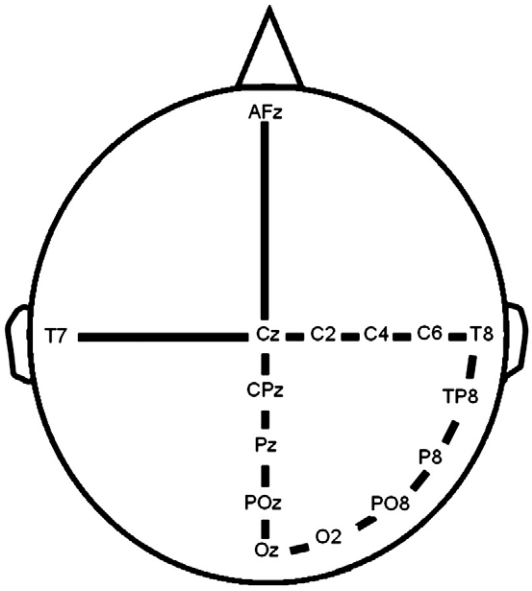

Fig. 7. Illustration of physical distances between sensor pairs used in accuracy study.

labeling purposes, i.e. the real coordinates of the electrodes are estimated in previous stages of the algorithm using the PCA technique.

Validation

Experiment I: phantom study

Sixty-four EEG sensors were taped onto a saline-filled MRI head phantom (Ø=190 mm, GE Healthcare, Milwaukee, US) (Fig. 6). Three additional sensors were taped onto the head phantom in order to define the fiducial points (nasion, left and right ears). All the sensors were placed according to the ten–ten system (Jasper, 1958, Oostenveld and Praamstra, 2001) (Fig. 4). For the EEG sensor localization, three different methods were used: i) 3D electromagnetic digitization (Polhemus, Inc., Colchester, VT), ii) manual MRI localization using ASA software (ANT, Enschede, NL) and iii) ALLES. For the manual localization, markers were positioned manually onto the images at the centers of the gadolinium balls. The marker positions were verified in axial, sagittal and coronal views of the MRI volume. Intra- and inter-observer measurements were made with manual MRI localization and electromagnetic digitization for all sixty-four sensors (five observers, four repetitions). To assess the accuracy of these three methods (i.e. electromagnetic digitization, manual MRI localization and ALLES), we measured fifteen physical distances between sensor pairs with a caliper (Digiroch®, 300 mm, 0.01 mm) (Fig. 7). Physical distances were chosen distributed along the anterior/posterior axis, along the right/left axis and along the temporal circumference. After the precision and reproducibility of this method had been validated in statistical tests, studies were carried out on epileptic patients in order to evaluate this new method in a real clinical setting.

Experiment II: studies with human subjects

We studied sixteen subjects (including 6 women). Ten were patients with medically intractable partial epilepsy and six were healthy volunteers. Mean age was 33.8 years old (range: 18–47). Informed consent was obtained from each subject, and the ethics committee (CCPPRB) of our Institution approved this study.

We taped sixty-four sensors, using collodion, onto the heads of the subjects, according to the ten–ten system (Fig. 8). High resolution EEG data were referenced to Fpz. The signal was recorded at a 1 kHz sampling rate (SD64 Headbox, Micromed, Italy). During sessions, the patients were relaxed and their eyes were closed. The patients were placed in a sound attenuated and electrically shielded room. The EEGs were recorded for 2 to 7 h. The subjects then immediately underwent MRI examination. For ten patients, electromagnetic digitization was performed twice by three different operators in order to estimate inter- and intra-observer measurements in clinical conditions. As in the phantom experiment, fifteen physical distances between the same pairs of sensors were measured with a caliper.

Error analysis and performance

We located the centroid of the marker on MR images (O') and the top of the electrode with the digitizer (O"), so the EEG sensor coordinates estimated with the manual MRI technique were corrected to account for this small displacement (Fig. 1A).

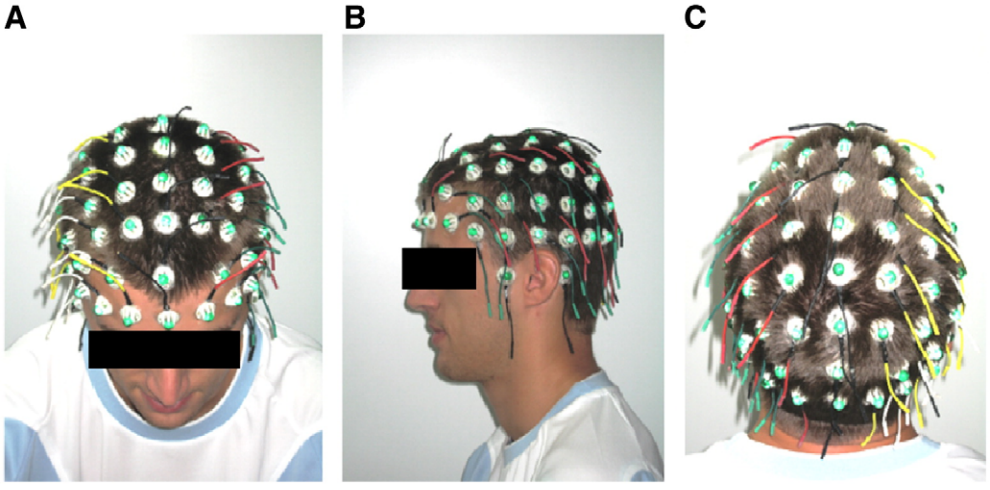

Fig. 8. Front (A) and left (B) and back (C) view of the 64 sensors on a patient's head.

Table 1
Inter-observer (A, B, C, D, E) accuracy in measuring scalp EEG sensors on the surface of the phantom scalp with manual MRI and with the electromagnetic digitization

Manual MRI	Mean	Std. Dev.	Minimum	Maximum
A	0.85	0.33	0.12	2.03
B	0.47	0.20	0.11	1.27
C	0.78	0.30	0.10	1.57
D	0.97	0.30	0.39	1.61
E	0.94	0.35	0.37	2.07
Digitizer	**Mean**	**Std. Dev.**	**Minimum**	**Maximum**
A	2.25	1.48	0.10	6.82
B	4.51	1.45	0.73	7.08
C	3.14	1.19	1.34	7.41
D	5.21	1.66	0.64	8.94
E	5.21	2.25	0.69	11.65

All numbers reported are in millimeters.

Since electromagnetic digitization is the commonest method for localizing EEG sensors, we decided to compare it with our method of MRI localization. In this study, two different parameters were estimated in order to validate our method of EEG sensor localization. First, we estimated the reproducibility of the measurement (intra- and inter-observer errors) and then the accuracy. In order to quantify the reproducibility, each set of coordinates was compared for calculating mean coordinates. Intra-class correlation coefficients and *t* test were calculated in order to compare electromagnetic digitization with MRI localization techniques.

To study the accuracy, the distances between sensors were calculated and compared with the Cartesian coordinates obtained with the electromagnetic digitizer, with manual MRI localization and ALLES. Intra-class correlation coefficients and *t* test were also calculated.

In order to assess the performance of automatic sensor localization and identification, we calculated for the patients the percentage of sensors correctly detected (true positive), the percentage of dots considered incorrectly as sensors (false positive) and the percentage of sensors not detected (false negative). Visual assessment of false positive and false negative was performed with the graphic user interface. Convex hull gives an excellent 3D visualization which allows detecting this sort of errors. We deleted dots corresponding to the false positive. False positives were clearly visually different from the markers. Dots which were not automatically detected (false negatives) were visually identified and manually added. Consequently all comparisons were done with 64 sensors.

Table 2
Distances measured with calipers and distances calculated with MRI (manual and ALLES) and electromagnetic digitizer coordinates

Distances	Calipers	Digitizer (mean)	Manual (mean)	ALLES
Cz–CPz	27.26	27.16	27.95	27.52
Cz–Pz	57.21	57.12	58.73	58.04
Cz–POz	81.77	81.93	83.36	82.52
Cz–Oz	109.80	111.27	105.40	104.29
T8–TP8	28.03	27.64	28.17	30.79
T8–P8	54.55	53.20	54.73	57.65
T8–PO8	77.94	75.26	77.96	82.24
T8–O2	101.88	97.10	101.72	105.67
T8–Oz	122.48	114.84	121.53	122.18
T8–C6	22.11	22.50	22.24	20.79
T8–C4	46.14	46.23	46.27	44.88
T8–C2	77.08	76.05	77.32	71.68
T8–Cz	102.20	99.76	102.45	98.35
Afz–Oz	164.76	162.09	162.27	160.45
T8–T7	167.28	159.98	169.39	167.57

Fifteen distances are represented along the anterior/posterior axis, along the left/right axis and around the circumference. All numbers reported are in millimeters.

Table 3
This table presents the differences between and *t* test values of all the methods of investigating distances

Differences	Mean (mm)	Std. Dev. (mm)	*t*	*p*
Cal. Dist.–Dig. Dist.	3.31	3.61	2.69	0.02
Cal. Dist.–MRI Dist.	1.00	1.20	0.13	0.90
Cal. Dist.–ALLES Dist.	2.54	1.85	0.47	0.65
MRI Dist.–Dig. Dist.	3.03	3.16	2.22	0.04

Cal.: calipers, Dig.: digitizer, MRI: magnetic resonance images, Dist.: distances, Std. Dev.: standard deviation.

Results

Phantom study

Inter- and intra-observer measurement errors are summarized in Table 1.

The composite (mean ± standard deviation) manual MRI inter-observer distance error was 0.80 ± 0.33 mm and 0.85 ± 0.33 mm for intra-observer distance error. The composite electromagnetic digitization inter-observer distance error was 4.21 ± 1.85 mm and 2.25 ± 1.48 mm for intra-observer distance error. We obtained a significant difference ($p < 0.01$) between manual MRI and electromagnetic digitization reproducibility. Physical distances, calculated MRI and digitizer distances are summarized in Table 2. The differences between these distances are presented in Table 3. The

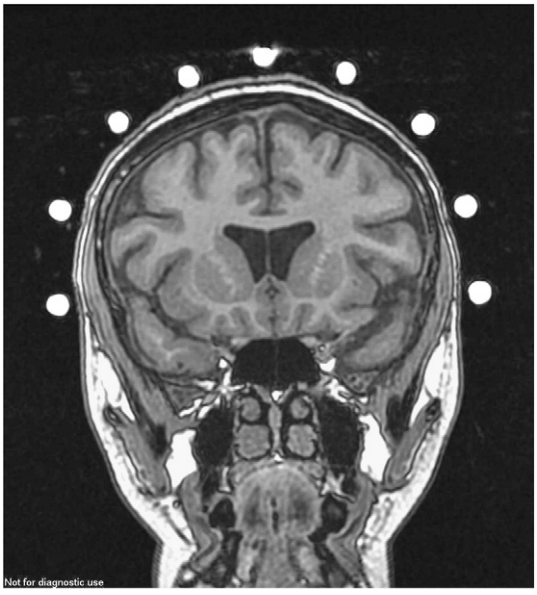

Fig. 9. Frontal view of EEG sensors on a patient's scalp.

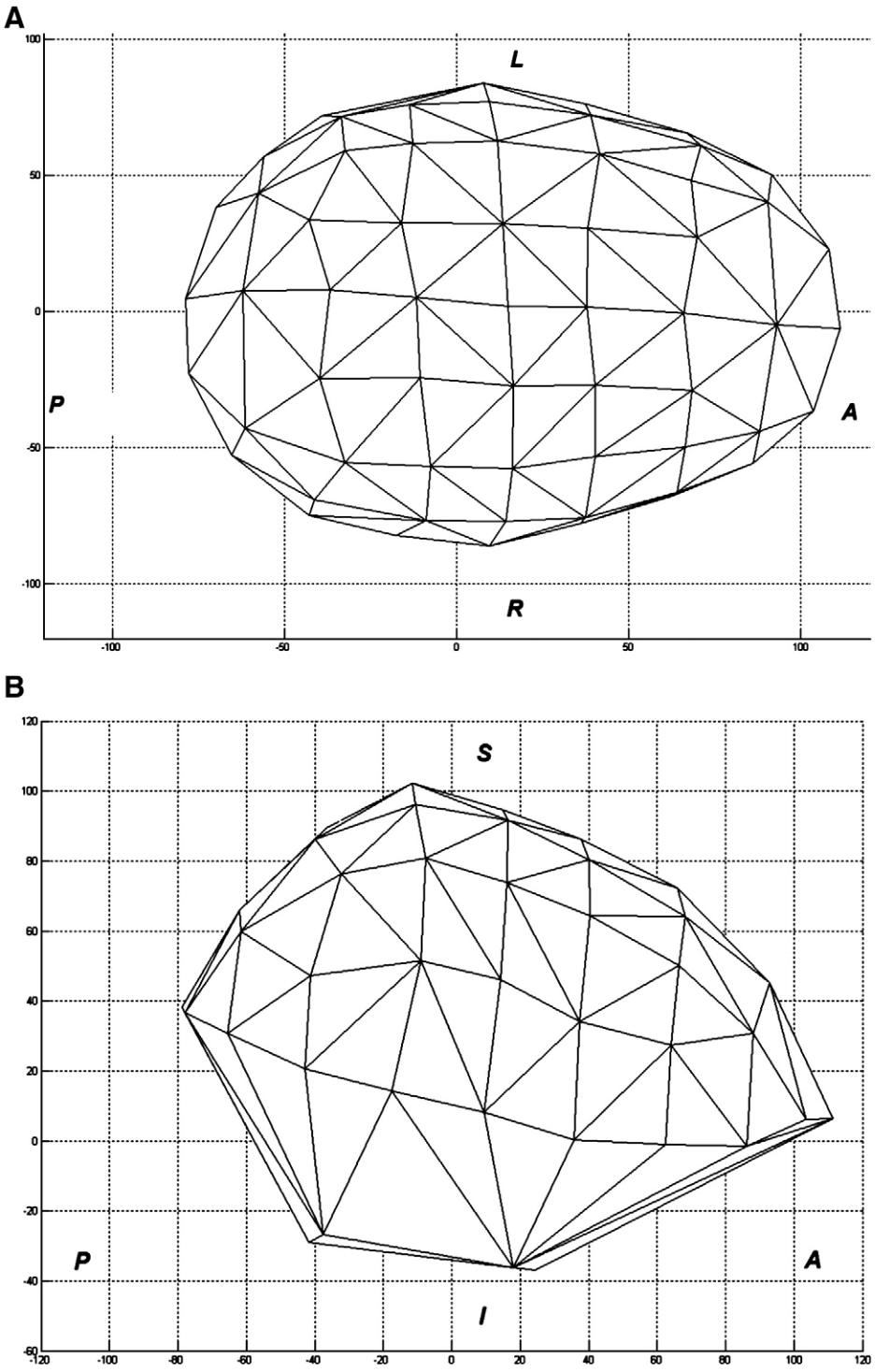

Fig. 10. 3D convex hull using the barycenters of the segmented Gado balls. Top sight (A) and right sight (B).

most important difference was noticed between the calipers and the electromagnetic digitization. This difference was about 3.31± 3.61 mm, whereas the difference between the calipers and ALLES was about 2.54±1.85 mm. There was a significant difference between the distances measured with calipers and the electromagnetic digitization (t=2.69, p=0.02) and between the distances measured with manual MRI and the electromagnetic digitization (t=2.22, p=0.04). No differences were seen between MRI (manual and ALLES) and the calipers (t<0.5).

Study with human subjects

Every subject underwent an MRI investigation with the new scalp EEG sensors (Fig. 9).

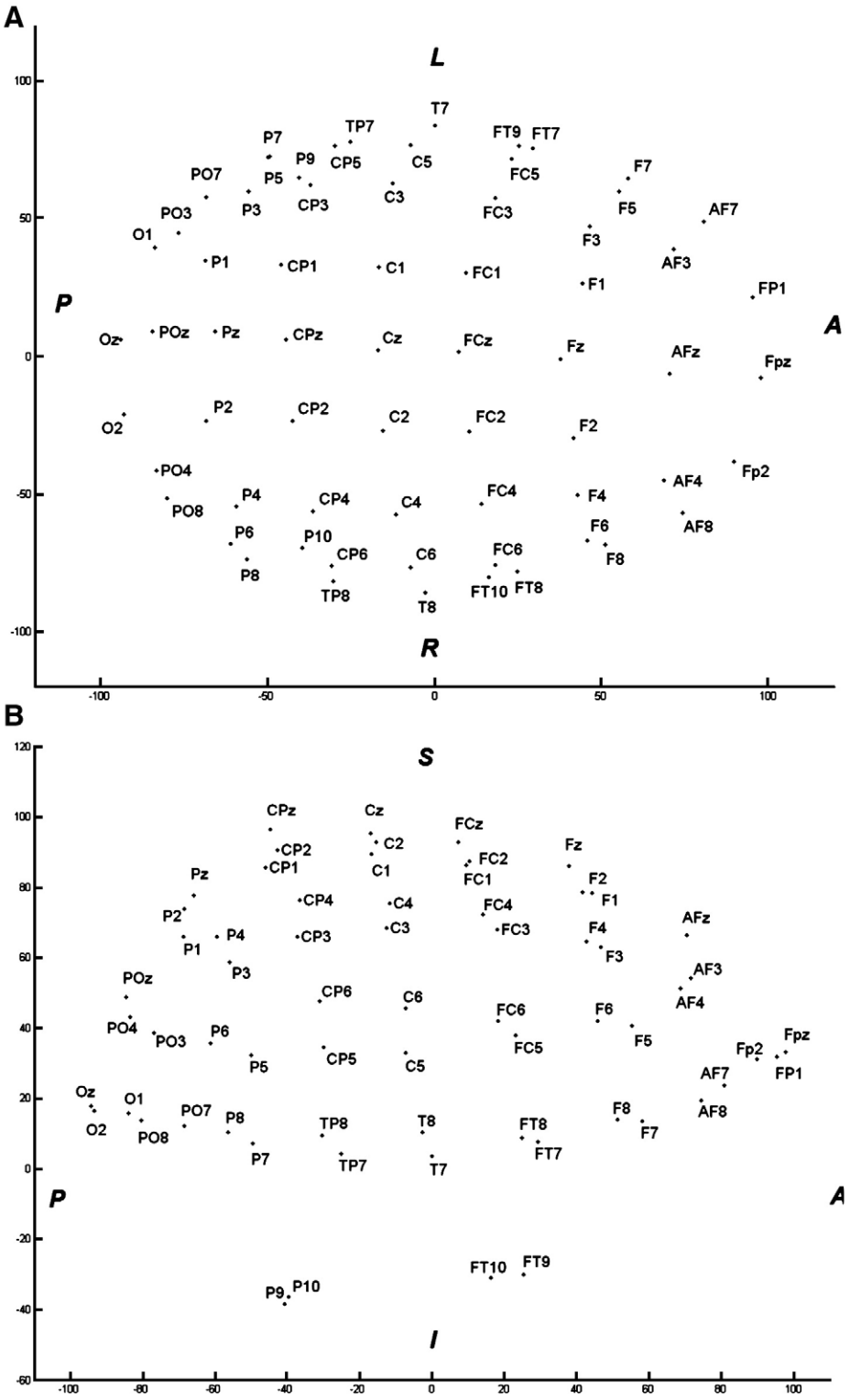

Fig. 11. Spatial reconstruction of the 64 sensors. Top sight (A) and right sight (B).

Examples of the 3D convex hull and spatial reconstruction of the 64 sensors are presented in Figs. 10 and 11. Each intersection of lines represents an EEG sensor. Inter- and intra-observer measurement errors are summarized in Table 4. The composite (mean±standard deviation) electromagnetic digitization inter-observer distance error was 4.17±2.10 mm and 2.59±1.07 mm for intra-observer distance error. In contrast to this, it is important to notice that there were no errors of reproducibility with the ALLES algorithm. In terms of accuracy, the correlation between fifteen physical distances measured to distances calculated with

Table 4
Inter- and intra-observer accuracy in measuring scalp EEG sensors on the surface of the patient's scalp with the digitizer

Subject	Inter-observer errors		Intra-observer errors	
	Mean	Std. Dev.	Mean	Std. Dev.
1	4.39	4.57	2.00	0.72
2	3.22	1.25	2.36	0.83
3	3.83	0.93	2.65	0.75
4	4.27	1.29	1.36	0.51
5	6.87	4.50	5.94	3.17
6	3.32	1.30	1.88	0.72
7	3.96	1.54	1.29	0.96
8	4.00	1.18	3.24	0.91
9	4.71	2.40	3.24	1.04
10	3.13	1.79	1.90	1.15

Digitizer measurements were made twice by three observers. All numbers reported are in millimeters.

ALLES and electromagnetic digitization is shown in Fig. 12. Excellent correlations were obtained between these three techniques. All intra-class correlations (ICC) were comprised between 0.97 and 0.99 R^2 correlation between physical distances measured with calipers and electromagnetic digitization was 0.99, 0.98 with calipers and ALLES and 0.97 with electromagnetic digitization and ALLES. All ALLES and electromagnetic digitization distances were compared with these physical distances. The mean and the standard deviation were calculated from the fifteen distances. The distance error with the digitizer was 2.18±1.60 mm (mean±standard deviation) and 2.91±2.29 mm with ALLES.

Performance of the automatic algorithm

Concerning the performance of the automatic algorithm, three different categories were identified: true positives, i.e. markers correctly detected and labeled, false negatives i.e. markers not detected and false positives, i.e. anatomical points wrongly considered as markers. The automatic algorithm presents an average of 91.6% true positives, 8.4% false negatives and 3.9% false positives.

Discussion

In this study, a new automatic method of EEG sensor localization was compared with a commonly used electromagnetic method. We have demonstrated that our automatic algorithm using MRI localization is better than the electromagnetic digitization in terms of precision with the phantom. Both methods are equally accurate with human subjects. This accuracy is within the range of precision currently required for dipole source imaging studies (Brinkmann et al., 1998). Spatial localization of EEG sensor is one step which can influence the source localization. Wang and Gotman, 2001 have described that for a noise-free signal, the source localization error due to electrode misplacement is about 2 mm, whereas it is about 5 mm for normal noisy signals. Moreover, he has clearly shown that at low signal noise ratio (SNR) levels, sensor misplacement has more effect on deep sources, whereas at high SNR levels, sensor misplacement has more effect on superficial sources. This is because noise has a greater effect on deep sources and is the dominant factor at low SNR levels. Others sources of errors can occur in source localization like uncertainties of the source models.

False negatives can be explained by the slice thickness which can reduce the volume and intensity of the markers. Moreover, a few gadolinium balls unfortunately burst during the tests. That explains false negative errors in the MRI localization of EEG sensors. This drawback can be solved by using a closed system that contains an MRI marker and an EEG electrode. This will also reduce the time devoted to visually inspecting images. It is important to notice that there is no error in labeling when all sensors were placed automatically. Concerning the false positives, it is possible to decrease it with the reduction of MRI volume. All false positives have appeared in the neck area. Furthermore, ALLES deletes automatically all dots included inside the convex hull. Only dots situated in the external surface of the head have been saved by ALLES.

ALLES makes the method completely reproducible and more useful for clinical application. This new automatic method is adapted to the international 10/10 configuration which is most widely used for high resolution EEG. However, it is possible to modify the reference model in the algorithm in order to detect and label another configuration of EEG sensors.

The method described in this paper is more robust than other previously reported methods (Gevins et al., 1990; Wang et al., 1996; Brinkmann et al., 1998; Yoo et al., 1997; Russell et al., 2005). No previous study that described MRI localization of electrodes used dedicated EEG sensors but all used a small number of MRI markers. Furthermore, all algorithms presented in the literature only detected EEG sensors whereas our algorithm automatically detects and labels EEG sensors. Consequently, the EEG sensor coordinates can be directly entered into source localization software. Each EEG acquisition is reviewed by experienced neurophysiologists. One limiting factor of automatic MRI localization is that the MRI must be done before removing these sensors.

Our EEG sensors present several advantages e.g. 1) the possibility of making long recordings (over several days) of high resolution EEG, which is currently not possible with the EEG cap. In this way, the probability of recording seizures is increased; 2)

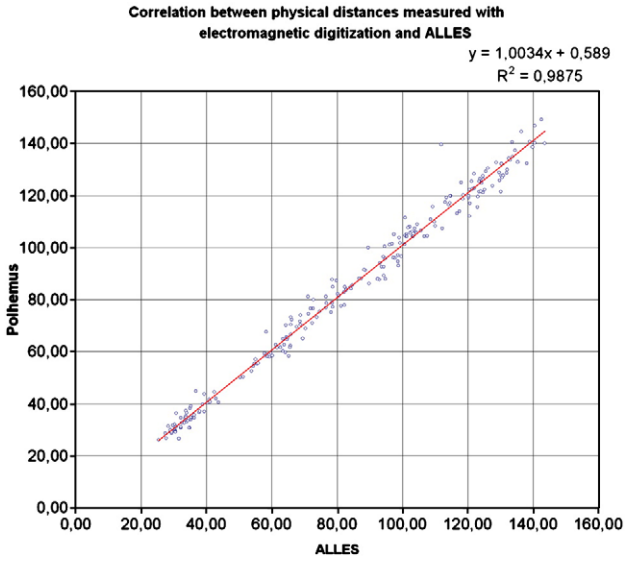

Fig. 12. Correlations between physical distances calculated with electromagnetic digitization and the ALLES method.

good fixation of the sensors during EEG acquisition. With EEG sensors glued onto the scalp, it is certain that they do not move; and 3) the EEG signals on each sensor are perfect because the sensor makes good contact with the scalp. With small sensor spacing, electrolyte dispersion can be a problem when a dense sensor array is used. In this study, it is important to notice that we do not have electrical bridging with our sensors. Moreover, if electrical bridging were present it would be easy to clean the skin. In contrast, using the EEG cap does not allow this procedure.

For future applications, it is clear that the automatic MRI algorithm must be associated with EEG/MRI sensors. Another application may be the localization of EEG sensors during simultaneous EEG/fMRI. This study demonstrates that better correlation of the anatomical position of EEG sensors can be achieved, for both clinical and research applications.

Acknowledgments

This study was supported by the company T.E.A, of Nancy, France and the Regional Council of Lorraine. The authors gratefully acknowledge the participation of the individuals involved in this study.

References

Alary, F., Doyon, B., Loubinoux, I., Carel, C., Boulanouar, K., Ranjeva, J.P., Celsis, P., Chollet, F., 1998. Event-related potentials elicited by passive movements in humans: characterization, source analysis, and comparison to fMRI. Neuroimage 8 (4), 377–390.

Boissonnat, J.-D., Teillaud, M., 1986. A hierarchical representation of objects: the Delaunay tree. Proc. 2nd Annu. ACM Sympos. Comput. Geom. pp. 260–268.

Brinkmann, B., O'Brien, T., Dresner, A., Lagerlund, T., Sharbrough, W.A., Robb, R., 1998. Scalp-recorded EEG localization in MRI volume data. Brain Topogr. 10 (4), 245–253.

De Munck, J.C., Vijn, P.C.M., Spekreijse, H., 1991. A practical method for determining electrode positions on the head. Electroenceph. Clin. Neurophysiol. 78, 85–87.

Ernst, P., Saias, I., Binhai, Z., 1996. Fast randomized point location without preprocessing in two- and three-dimensional Delaunay triangulations. Proc. 12th Annu. ACM Sympos. Comput. Geom., pp. 274–283.

Gavaret, M., Badier, J.M., Marquis, P., Bartolomei, F., Chauvel, P., 2004. Electric source imaging in temporal lobe epilepsy. J. Clin. Neurophysiol. 21 (4), 267–282.

Gavaret, M., Badier, J.M., Marquis, P., McGonigal, A., Bartolomei, F., Regis, J., Chauvel, P., 2006. Electric source imaging in frontal lobe epilepsy. J. Clin. Neurophysiol. 23 (4), 358–370.

Gevins, A., Brickett, P., Costales, B., Le, J., Reutter, B., 1990. Beyond topographic mapping: towards functional–anatomical imaging with 124-channel EEGs and 3-D MRIs. Brain Topogr. 3 (1), 53–64.

Guofei, Hu, Jie, Xu, Lanfang, Miao, Qunsheng, Peng, 2005. Bilateral estimation of vertex normal for point-sampled models. Lect. Notes Comput. Sci. 758–768.

Heijmans, H.J.A.M., 1994. Morphological image operators. Advances in Electronics and Electron Physics. Academic Press, Boston.

Huppertz, H.J., Hof, E., Klish, J., Wagner, M., Lucking, C.H., Kristeva-Feige, R., 2001. Localization of interictal delta and epileptiform EEG activity associated with focal epileptogenic brain lesions. Neuroimage 13 (1), 15–28.

Jasper, H.H., 1958. The ten–twenty electrode system of the international federation. Electroencephalogr. Clin. Neurophysiol. 10, 367–380.

Khosla, D., Don, M., Kwong, B., 1999. Spatial mislocalization of EEG electrodes — effects on accuracy of dipole estimation. Clin. Neurophysiol. 110, 261–271.

Koessler, L., Maillard, L., Benhadid, A., Vignal, J.P., Braun, M., Vespignani, H., 2007. Spatial localization of EEG electrodes. Neurophysiologie Clinique/Clin. Neurophysiol. 37, 97–102.

Lagerlund, T., Sharbrough, F., Jack Jr, C., Erickson, B., Strelow, D., Cicora, K., Busacker, N., 1993. Determination of 10/20 system electrode locations using magnetic resonance image scanning with markers. Electroenceph. Clin. Neurophysiol. 86, 7–14.

Lantz, G., Grave de Peralta, R., Spinelli, L., Seeck, M., Michel, C.M., 2003. Epileptic source localization with high density EEG: how many electrodes are needed? Clin. Neurophysiol. 114, 63–69.

Le, J., Lu, M., Pellouchoud, E., Gevins, A., 1998. A rapid method for determining standard 10/10 electrode positions for high resolution EEG studies. Electroenceph. Clin. Neurophysiol. 106, 554–558.

Michel, C.M., Murray, M.M., Lantz, G., Gonzalez, S., Spinelli, L., Grave de Peralta, R., 2004. EEG source imaging. Clin. Neurophysiol. 115 (10), 2195–2222.

Oostenveld, R., Praamstra, P., 2001. The five percent electrode system for high-resolution EEG and ERP measurements. Clin. Neurophysiol. 112, 713–719.

Russell, G.S., Eriksen, K.J., Poolman, P., Phan, Luu, Tucker, Don M., 2005. Geodesic photogrammetry for localizing sensor positions in dense-array EEG. Clin. Neurophysiol. 116 (5), 1130–1140.

Sijbers, J., Vanrumste, B., Van Hoey, G., Boon, P., Verhoye, M., Van der Linden, A., Van Dyck, D., 2000. Automatic localization of EEG electrode markers within 3D MR data. Magn. Reson. Imaging 18, 485–488.

Steddin, S., Bötzel, K., 1995. A new device for scalp electrode localization with unrestrained head. J. Neurol. 242, 65.

Thees, S., Blankenburg, F., Taskin, B., Curio, G., Villringer, A., 2003. Dipole source localization and fMRI of simultaneously recorded data applied to somatosensory categorization. Neuroimage 18 (3), 707–719.

Tucker, D.M., 1993. Spatial sampling of head electrical fields: the geodesic sensor net. Electroenceph. Clin. Neurophysiol. 87, 154–163.

Wang, Y., Gotman, J., 2001. The influence of electrode location errors on EEG dipole source localization with a realistic head model. Clin. Neurophysiol. 112, 1777–1780.

Wang, Y., Maurer, C., Fitzpatrick, J., 1996. An automatic technique for finding and localizing externally attached markers in CT and MR volume images of the head. IEEE Trans. Biomed. Eng. 43 (6), 627–637.

West, J., Fittzpatrick, M., Wang, M.Y., Dawant, M.B., Maurer, C.R., Kessler, R.M., Woods, R.P., 1997. Comparison and evaluation of retrospective intermodality image registration techniques. J. Comput. Assist. Tomograph. 21, 554–566.

Yoo, S.-S., Guttmann, C., Ives, J., Panych, L., Kikinis, R., Schomer, D., Jolesz, F., 1997. 3D localization of surface 10–20 EEG electrodes on high-resolution anatomical MR images. Electroenceph. clin. Neurophysiol. 102, 335–339.